Magnetic properties of FeAl₂ and Fe₂Al₅

Z. Jagličić,[1] S. Vrtnik,[2] M. Feuerbacher,[3] and J. Dolinšek[2,4,*]

[1]*Institute of Mathematics, Physics and Mechanics & University of Ljubljana, Faculty of Civil and Geodetic Engineering,*
Jamova 2, SI-1000 Ljubljana, Slovenia
[2]*Jozef Stefan Institute & University of Ljubljana, Faculty of Mathematics and Physics, Jamova 39, SI-1000 Ljubljana, Slovenia*
[3]*Institut für Festkörperforschung, Forschungszentrum Jülich, D-52425 Jülich, Germany*
[4]*EN–FIST Centre of Excellence, Dunajska 156, SI-1000 Ljubljana, Slovenia*

We have investigated magnetic properties of the FeAl₂ and Fe₂Al₅ intermetallic compounds. By measuring the zero-field-cooled and field-cooled static (dc) magnetic susceptibilities in low and high magnetic fields, the frequency-dependent (ac) susceptibility, the magnetization versus the magnetic field, and the thermoremanent magnetization time decay, we found that the magnetic structures of FeAl₂ and Fe₂Al₅ are richer than those published so far in the literature. FeAl₂ undergoes complex two-step magnetic ordering. At $T \approx 32$ K, a magnetic phase transition (not yet specified) takes place in which a small fraction of the Fe spins participate, whereas at $T_{f2} \approx 12$ K, the majority spin fraction undergoes a spin-freezing transition to a spin glass phase. Fe₂Al₅ undergoes a transition to a spin glass phase at the spin freezing temperature $T_f \approx 3$ K, which was not reported previously. The spin glass phase in Fe₂Al₅ is "soft" and fragile with respect to the external magnetic field and can only be observed in low magnetic fields below $\sim$100 Oe. The origins of the spin glass ordering in the FeAl₂ and Fe₂Al₅ phases are randomness and frustration that are present on the Fe sublattices of both compounds. In FeAl₂, the Fe spins are positioned randomly on the three mixed-occupation Al/Fe sites of the unit cell, whereas in Fe₂Al₅, partial occupation of the Fe-neighboring Al2 and Al3 atomic sites imposes different degrees of Fe moment screening by the electron cloud, resulting in a random distribution of the magnetic moment sizes. Geometric frustration because of positioning of the antiferromagnetically coupled Fe spins on triangles is present in both compounds as well.

I. INTRODUCTION

The structurally complex alloy phases in the $Fe_{1-x}Al_x$ system have attracted a lot of interest regarding their rich variety of magnetic properties. Although the vanishing of magnetic moments of diluted Fe impurities in the Al metal host was investigated in detail,[1,2] less is known about the magnetic structures of the phases with the Fe concentration away from the isolated-impurity limit. On the iron-rich side of the Fe–Al phase diagram, the magnetic structures of the $Fe_{70}Al_{30}$ compound were reported to include ferromagnetic (FM), superparamagnetic, and spin glass-type orderings in different temperature ranges below 400 K.[3,4] The $Fe_{1-x}Al_x$ phases on the aluminum-rich side of the phase diagram were investigated to a lesser extent. A spin glass phase was reported for the FeAl₂ compound below the spin-freezing temperature $T_f = 35$ K,[5,6] whereas Fe₂Al₅ and Fe₄Al₁₃ were reported to be Curie-type paramagnets down to the lowest investigated temperature of 2 K.[7–9] The magnetic susceptibilities of FeAl₂ and Fe₂Al₅ were investigated in magnetic fields of $H = 1$ kOe[5,8] and $H = 8$–17.5 kOe,[7] which were strong enough that some "soft" and fragile internal magnetic structures could already be destroyed and polarized by the external field. In this paper we revisit the magnetic properties of the FeAl₂ and Fe₂Al₅ compounds. By measuring the zero-field-cooled (zfc) and field-cooled (fc) static (dc) magnetic susceptibilities in low and high magnetic fields and combining these with measurements of the magnetization versus the magnetic field $M(H)$, the frequency-dependent (ac) susceptibility $\chi'(\omega)$, and the thermoremanent magnetization (TRM) time decay as a function of the aging time $M_{TRM}(t_w)$ and the aging magnetic

field, $M_{TRM}(H_{fc})$, we show that the magnetic structures of FeAl₂ and Fe₂Al₅ are richer than those published so far in the literature. In particular, FeAl₂ undergoes a two-step magnetic ordering upon cooling with an additional spin-freezing temperature at $T_{f2} \approx 12$ K, whereas the upper transition at $T \approx 32$ K appears more like a thermodynamic phase transition than spin glass freezing. Fe₂Al₅, on the other hand, undergoes a transition to a spin glass phase at $T_f \approx 3$ K, which was not reported previously.

II. STRUCTURAL CONSIDERATIONS AND SAMPLE PREPARATION

A. FeAl₂

The structure of FeAl₂ has been investigated by several authors.[10–14] In our analysis we consider the most recent study by Stein *et al.*[14] FeAl₂ has a triclinic unit cell with $a = 4.87$Å, $b = 6.45$Å, $c = 8.77$Å, $\alpha = 91.9°$, $\beta = 73.3°$, and $\gamma = 96.8°$ (space group $P1$). The unit cell contains 18 crystallographic sites, including 10 Al sites, 5 Fe sites, and 3 sites with mixed Al and Fe occupation (labeled as M1, M2, and M3) in the proportion 0.67Al + 0.33Fe. The structure is an irregular close-packed arrangement. Further structural details related to the magnetic properties of the FeAl₂ phase (the analysis of the Fe sublattice) are given in the discussion.

Our sample was a polygrain material, prepared by direct alloying and annealed at 950 °C for 290 h. A rectangular bar of $3 \times 3 \times 5$ mm³ was cut from the parent ingot. Its composition (as an atomic percentage) was $Fe_{32.8}Al_{67.2}$, corresponding to the formula FeAl₂.₀₅. The backscattered-electron scanning

(a) FeAl$_2$

Al2Fe-rod 950C 290h 25.0kV x55 200µm

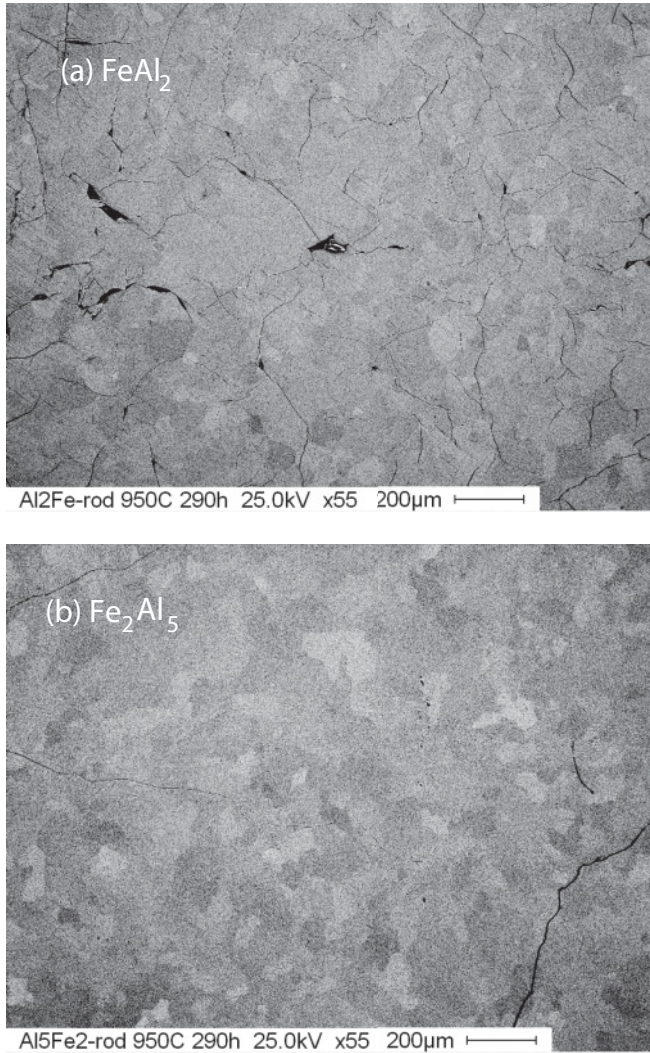(b) Fe$_2$Al$_5$

Al5Fe2-rod 950C 290h 25.0kV x55 200µm

FIG. 1. (a) The SEM backscattered-electron micrograph of the FeAl$_2$ material, annealed at 950 °C for 290 h. The residual contrast results from the grain structure of the polycrystalline material. The brittle material shows a high density of cracks on the 200-μm scale, formed by thermal contraction during cooling of the as-cast material. Some holes are observed as dark features as well. (b) A SEM backscattered-electron micrograph of the Fe$_2$Al$_5$ material, annealed at 950 °C for 290 h. The brittle material shows cracks, although they have a smaller density than in FeAl$_2$.

electron microscope (SEM) micrograph [Fig. 1(a)] reveals that the material was single phased. The image still shows slight contrast, but within the accuracy of the measurement this is not caused by the presence of other phases; rather, it reflects the grain structure of the polycrystalline material. The brittle material exhibited a high density of cracks on the 200-μm scale, formed by thermal contraction during cooling of the as-cast material. Some holes are observed as dark features as well.

B. Fe$_2$Al$_5$

According to Burkhardt *et al.*,[15] Fe$_2$Al$_5$ has an orthorhombic unit cell with $a = 7.66$Å, $b = 6.42$Å, and $c = 4.22$Å (space group *Cmcm*). The unit cell contains a single crystallographic

Fe site (four per cell) and three Al sites. The site Al1 (eight per cell) is fully occupied, while the sites Al2 (four per cell) and Al3 (eight per cell) are too close to each other to be occupied simultaneously, resulting in their partial occupation factors of 0.36 and 0.23, respectively. The structure is a three-dimensional framework with channels in the shape of stacked pentagonal antiprisms along the [001] axis. The Al2 and Al3 sites make up disordered chains along [001]. Further structural details related to the magnetic properties of the Fe$_2$Al$_5$ phase (the analysis of the Fe sublattice) are given in the discussion.

Our sample was a polygrain material, prepared by direct alloying and annealed at 950 °C for 290 h. A rectangular bar of $3 \times 3 \times 8$ mm^3 was cut from the parent ingot. Its composition (as an atomic percentage) was Fe$_{27.3}$Al$_{72.7}$, corresponding to the formula Fe$_2$Al$_{5.3}$ that is within the reported composition range of the Al$_2$Fe$_5$ phase.[16,17] The backscattered-electron SEM micrograph [Fig. 1(b)] reveals that the material was single phased. The remaining contrast on the image again reflects the grain structure of the polycrystalline material. The brittle material exhibited cracks, although these are of smaller density than those in FeAl$_2$.

III. MAGNETIC PROPERTIES OF FeAl$_2$

A. Zero-field-cooled and field-cooled magnetic susceptibilities

Magnetic measurements were conducted using a Quantum Design MPMS XL-5 SQUID magnetometer equipped with a 50-kOe magnet, operating in the temperature range 1.9–400 K. In the first set of measurements, the zfc and fc dc magnetic susceptibilities $\chi = M/H$ of FeAl$_2$ were determined in the temperature range 1.9–300 K in magnetic fields $H = 50$ and 100 Oe and $H = 1$ and 10 kOe [Fig. 2(a)]. Both χ_{zfc} and χ_{fc} show an inflection-point-type anomaly of $\sim$32 K (marked by an arrow). χ_{zfc} shows an additional maximum at 12 K, whereas χ_{fc} continues to increase below that temperature. For all investigated fields, a zfc–fc susceptibility splitting is observed up to the highest investigated temperature of 300 K, demonstrating the presence of a magnetically ordered spin fraction up to room temperature. At temperatures above the anomaly at 32 K, the magnetization of the magnetically ordered spin fraction is very small and largely independent of the external magnetic field so that when it is divided by the magnetic field to calculate the susceptibility $\chi = M/H$ it becomes increasingly less visible. On the scale of Fig. 2(a), the zfc–fc splitting is clearly observed only for the lower fields of 50 and 100 Oe, whereas it becomes unobservable (except below the maximum in χ_{zfc} upon $T \rightarrow 0$) for the fields of 1 kOe and higher. In Fig. 2(b), χ_{zfc} and χ_{fc} in the field $H = 1$ kOe are shown on an expanded scale in the low-temperature region below 40 K. We observe that the zfc–fc splitting increases significantly just below the anomaly at 32 K but remains small and almost temperature independent down to the maximum in χ_{zfc} at 12 K. Below the χ_{zfc} maximum, the zfc–fc splitting increases drastically upon further cooling.

Although the temperature-dependent variation of the zfc–fc susceptibility splitting below the anomaly at 32 K can be attributed to the complex magnetic features of the FeAl$_2$ phase, the origin of the tiny magnetically ordered spin fraction in the high-temperature region between room temperature and 32 K
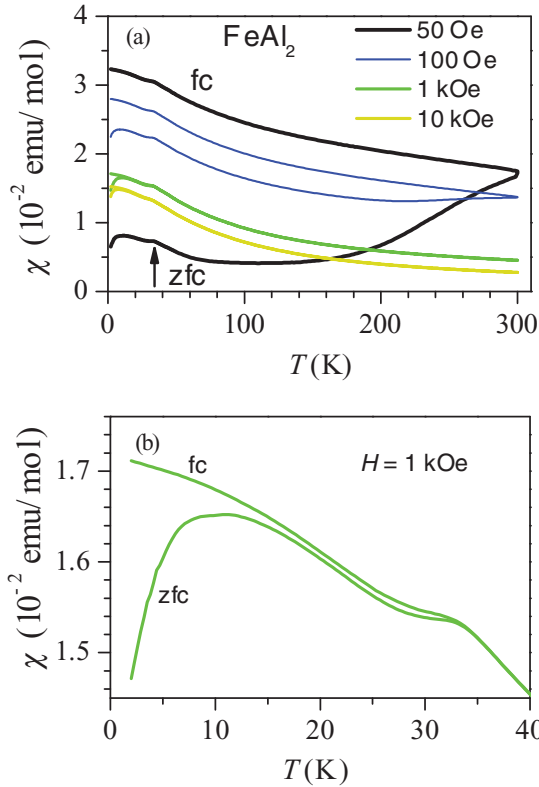
FIG. 2. (Color online) (a) The zfc and fc dc magnetic susceptibilities $\chi = M/H$ of FeAl$_2$ in the temperature range 1.9–300 K in the magnetic fields $H = 50$ and 100 Oe and $H = 1$ and 10 kOe. The temperature $T = 32$ K of the inflection-point-type anomaly observed in both χ_{zfc} and χ_{fc} is marked by an arrow. (b) χ_{zfc} and χ_{fc} in the field $H = 1$ kOe on an expanded scale in the low-temperature region below 40 K.

is not clear. Nevertheless, it should be presumably associated with defects in the material. The SEM and x-ray diffraction (XRD) characterization did not reveal the presence of any secondary phases above the detection limit of these methods. A probable explanation is found in the Fe-rich spin clusters at the surface of the cracks [the investigated material exhibited a high density of cracks, as shown in Fig. 1(a)], where the FeAl$_2$ stoichiometry is locally corrupted and the reduced Al coordination around the Fe atoms promotes magnetic moment formation. Tiny amounts of the Fe–O FM surface oxides, not detectable by XRD, cannot be excluded either. The surface iron oxides in the Fe-containing intermetallics are inevitable at ambient conditions; if polished away, they reappear almost instantly in the air atmosphere.

B. Paramagnetic susceptibility

The analysis of the susceptibility $\chi(T)$ in the high-temperature paramagnetic regime was performed assuming validity of the Curie-Weiss law

$$\chi = \chi_0 + \frac{C}{T - \theta}, \qquad (1)$$

where χ_0 is the temperature-independent part of the susceptibility, C the Curie-Weiss constant and θ the Curie-Weiss temperature. The constant C gives information on the
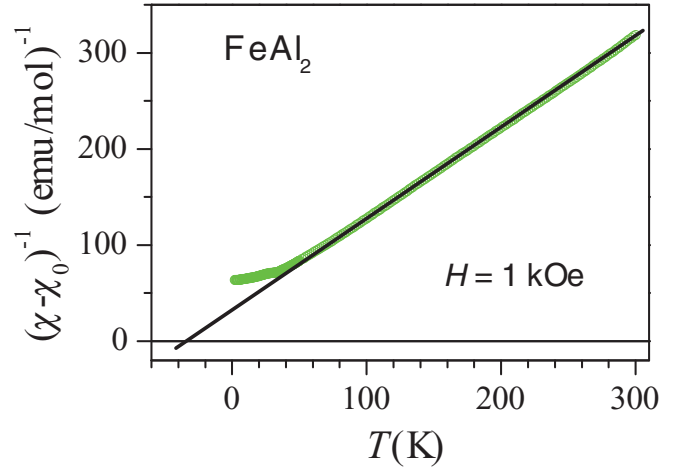

FIG. 3. (Color online) Magnetic susceptibility of FeAl$_2$ in $H = 1$ kOe in a $(\chi - \chi_0)^{-1}$ versus temperature plot. The solid line is the Curie-Weiss fit with Eq. (1) of the high-temperature data $T > 80$ K. The fit parameters are given in the text.

magnitude of the Fe moments, whereas the type and strength of the coupling between the moments can be estimated from the sign and magnitude of θ. The analysis was performed on the susceptibility data measured in $H = 1$ kOe, where the tiny zfc–fc splitting in the paramagnetic regime above the anomaly at 32 K is no more observable on the scales of Fig. 2(a) and Fig. 2(b). The $(\chi - \chi_0)^{-1}$ versus temperature plot is shown in Fig. 3. The fit of the high-temperature data for $T > 80$ K (solid line) yielded the parameter values $\chi_0 = 1.4 \times 10^{-3}$ emu/mol, $C = 1.05$ emu K/mol, and $\theta = -35$ K. The negative Curie-Weiss temperature suggests an antiparallel—i.e., an antiferromagnetic (AFM) type—coupling between the spins. χ_0 is generally a sum of the Larmor diamagnetic susceptibility because of the atomic cores χ_{dia} and the susceptibility of conduction electrons (the Pauli paramagnetic spin susceptibility and the Landau orbital diamagnetic susceptibility), where all contributions are of the same order of magnitude. Considering the Fe^{2+} and Fe^{3+} valence states, the χ_{dia} contribution was calculated from literature tables[18] to be in the range $\chi_{dia} = (-1.4, -1.7) \times 10^{-5}$ emu/mol. The fit-determined χ_0 value is 100 times larger than $|\chi_{dia}|$, showing that a small FM contribution (the one responsible for the tiny zfc–fc susceptibility splitting up to room temperature) is present in the signal of the paramagnetic phase.

The value of the Curie constant C was used to calculate the mean effective magnetic moment $\bar{\mu}_{eff} = \bar{p}_{eff}\mu_B$ per Fe ion, where $\bar{p}_{eff}$ is the mean effective Bohr magneton number that can be calculated using the formula[19] $\bar{p}_{eff} = 2.83\sqrt{C}$ (with C given in units per mol of Fe atoms). We obtain $\bar{p}_{eff} = 2.9$ per Fe atom. Comparison of this value to the Bohr magneton numbers of the bare Fe^{2+} and Fe^{3+} ions ($p = 5.4$ and 5.9, respectively) demonstrates that the Fe moments in the FeAl$_2$ phase are partially screened by the conduction-electron cloud in a conducting environment. The values for $\bar{p}_{eff}$ and θ of our sample are close to the values determined for FeAl$_2$ by Lue et al.,[5] who reported $\bar{p}_{eff} = 2.55$ and $\theta \approx -42$ K.
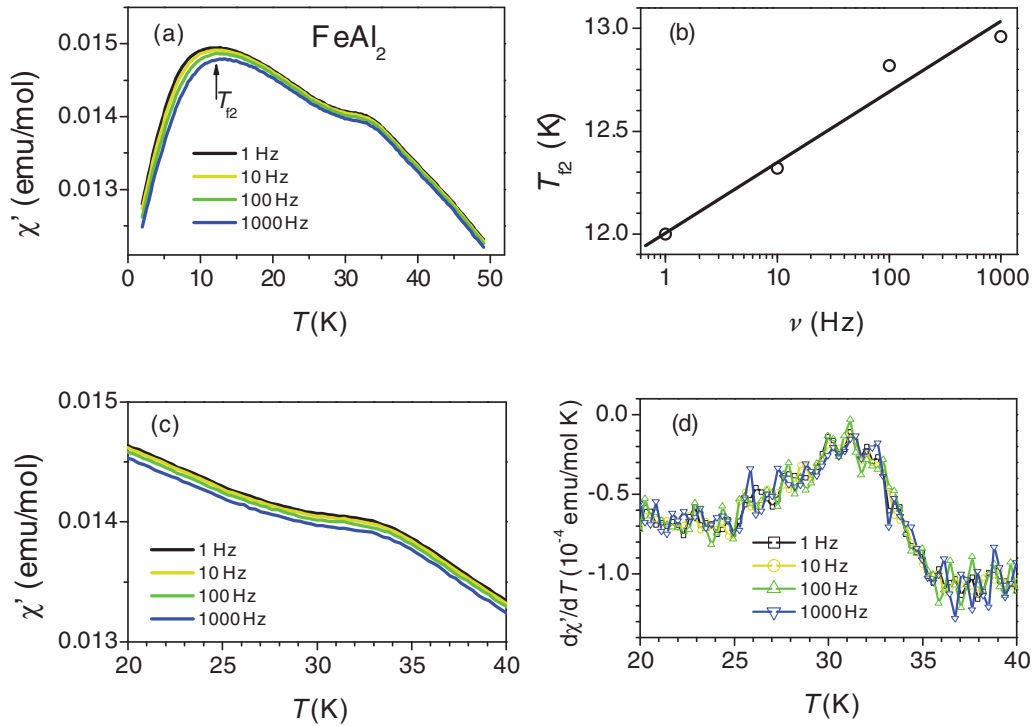
FIG. 4. (Color online) (a) Real part χ' of the ac susceptibility of $FeAl_2$ measured in an ac magnetic field of the amplitude $H_0 = 6.5$ Oe at frequencies $\nu = 1$, 10, 100, and 1000 Hz. T_{f2} is marked by an arrow. (b) Frequency dependence of the temperature T_{f2} of the maximum in χ'. A solid line was used to evaluate the relative change of T_{f2} per decade ν, $\Delta T_{f2}/T_{f2}\Delta (\log \nu) = 0.028$. (c) An expanded portion of χ' around the anomaly at $T \approx 32$ K. (d) Derivatives $d\chi'(\nu)/dT$ of the curves displayed in (c), showing no noticeable shift of the maximum (occurring at the inflection point in χ') with the frequency.

C. Ac susceptibility

The ac susceptibility was measured in an ac magnetic field of the amplitude $H_0 = 6.5$ Oe at the frequencies $\nu = 1$, 10, 100, and 1000 Hz. The real part χ' of the susceptibility is displayed in Fig. 4(a). χ' shows a cusp at $T \approx 12$ K and an inflection point at $T \approx 32$ K. The position of the cusp is frequency dependent, shifting to lower temperatures at lower frequencies. By considering the cusp in χ' as though it occurred at the spin-freezing temperature T_{f2}, below which the ergodicity of the spin system is broken on the experimental time scale, the $T_{f2}(\nu)$ relation was determined from the $\chi'(\nu)$ curves. The $T_{f2}(\nu)$ graph is shown in Fig. 4(b), where a logarithmic dependence (base 10) on the frequency is evident. At the lowest frequency, the cusp occurs at the temperature $T_{f2}(1\ \text{Hz}) = 12.0$ K, whereas at the highest frequency it occurs at $T_{f2}(1\ \text{kHz}) = 13.0$ K. The frequency shift of the freezing temperature is often evaluated quantitatively by the empirical criterion $\Delta T_{f2}/T_{f2}\Delta (\log \nu)$, i.e., by calculating the relative change of T_{f2} per decade ν. For $FeAl_2$, this ratio equals 0.028, which is in the range found for canonical spin glasses[20] like AuFe and PdMn. This classifies the spin-freezing transition at $T_{f2} \approx 12$ K as being of spin glass type.

The frequency dependence of the inflection-point anomaly at $T \approx 32$ K is more subtle. The zoomed-in part of the ac susceptibility $\chi'(\nu)$ around the anomaly is shown in Fig. 4(c). In the absence of a clear local maximum, no conclusions on the possible shift of the anomaly with the frequency can be drawn. At the inflection point, the first derivative $d\chi'/dT$ shows a maximum (for the negative-sloping χ'), so we have calculated the derivatives of all $\chi'(\nu)$ curves to see whether the maximum

shifts with the frequency. The $d\chi'(\nu)/dT$ curves are displayed in Fig. 4(d), showing no noticeable shift of the maximum with the frequency. This indicates that the anomaly at $T \approx 32$ K is not of spin glass freezing type but rather is a thermodynamic phase transition that is characterized by a frequency-independent anomaly in the ac susceptibility. Hence, the designation of the anomaly temperature $T \approx 32$ K as the "freezing temperature"[5] in the sense of the spin glass-type gradual spin freezing does not seem to be appropriate; rather, it should be considered as a temperature of a kind of magnetic phase transition, not yet specified, in which a fraction of the Fe spins participate. This is further corroborated by the zfc–fc dc susceptibility splitting of Fig. 2(b) increasing rather suddenly just below the anomaly point at $T \approx 32$ K but then rapidly saturating and remaining almost constant down to the freezing temperature $T_{f2} \approx 12$ K. Such behavior is typical for a phase transition and is in contrast to the gradual spin freezing, where the zfc–fc susceptibility splitting increases continuously upon cooling below the spin freezing temperature. The spin ordering in the $FeAl_2$ phase thus appears to be a two-step process: (1) a small fraction of spins undergo a kind of magnetic phase transition at $T \approx 32$ K, and (2) the majority of spins undergo spin glass freezing below $T_{f2} \approx 12$ K.

D. Magnetization versus magnetic field

The $M(H)$ curves were recorded at the temperatures 2, 5, and 10 K. The curves differ noticeably only in the hysteretic region around the $H = 0$ origin. Therefore, in Fig. 5(a) we
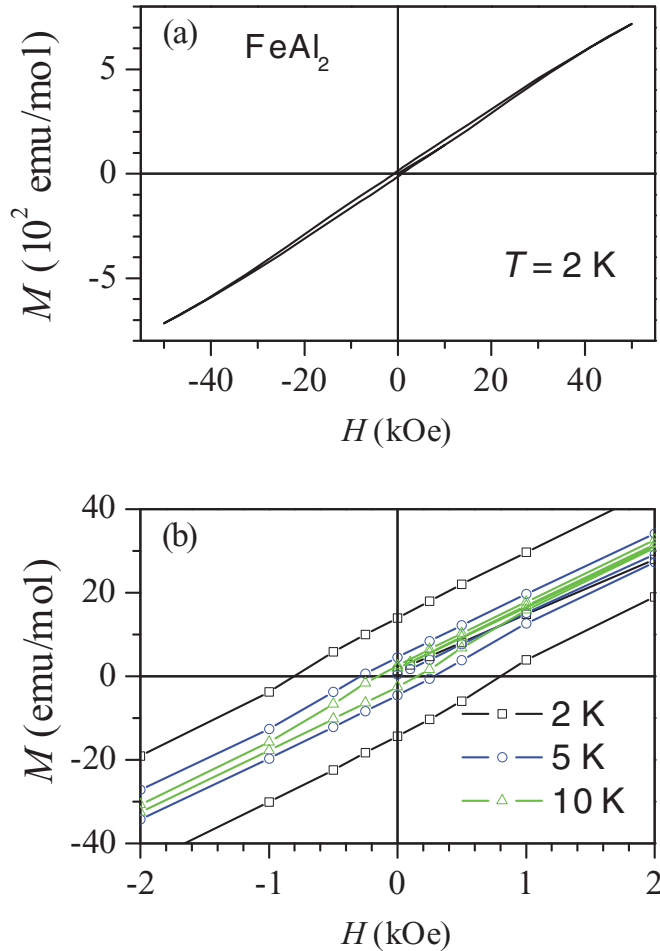
FIG. 5. (Color online) (a) $M(H)$ hysteresis loop of FeAl$_2$ at $T = 2$ K for the field sweep ± 50 kOe. (b) The zoomed-in parts of the hysteretic region around $H = 0$ for the temperatures 2, 5, and 10 K.

display the full curve only for $T = 2$ K, whereas in Fig. 5(b) the zoomed-in parts of the hysteretic region for all temperatures are shown. The $M(H)$ curves are linearlike (of the AFM type) in the magnetic field up to the highest investigated field of ± 50 kOe. The $M(H)$ hysteresis loop at $T = 2$ K of Fig. 5(a) remains open up to ~30 kOe, classifying it as an AFM-type hysteresis (a typical FM loop saturates quite rapidly for much lower fields of a few kilo-oersteds only). Perfectly compensated AFMs do not show hysteresis, indicating the presence of uncompensated AFM-coupled spins. Such a situation is encountered in uncompensated AFMs but is also typical for spin glasses. The coercive field at 2 K is $H_c^{2\text{K}} = 800$ Oe. At the two higher investigated temperatures of 5 K and 10 K, the coercive field diminishes rapidly, amounting to $H_c^{5\text{K}} = 280$ Oe and $H_c^{10\text{K}} = 140$ Oe, respectively. Pronounced hysteretic behavior of the spin system is thus observed only deeply below the spin freezing temperature T_{f2}.

E. Thermoremanent magnetization

A spectacular manifestation of the spin freezing dynamics and nonergodicity in magnetically frustrated systems like spin glasses is the observation of aging effects in the ultraslow TRM time decay.[21,22] In a TRM-decay experiment, the researcher cools the sample in a field H_{fc} from above the spin-freezing temperature T_{f} to a measuring (and, at the same time, aging) temperature $T_1 < T_{\text{f}}$, where the spin system is allowed to age for a time t_w. After t_w, the field H_{fc} is cut to zero and the magnetization time decay is measured over macroscopic times. Upon $H_{\text{fc}} \to 0$, the reversible part of the fc magnetization M_{fc} decays to zero almost instantaneously, whereas the irreversible part (the TRM) decays very slowly, typically much slower than any experimentally accessible observation time. TRM is a fraction of M_{fc} before the field H_{fc} is cut to zero, and depending on temperature, its magnitude is from a few percent up to the almost full M_{fc}. The TRM decay depends on the aging temperature T_1, the aging time t_w, and the field H_{fc} in which the aging is performed.

In the first set of experiments (TRM versus T_1), the sample was cooled in the field $H_{\text{fc}} = 100$ Oe from room temperature to different measuring temperatures: (1) $T_1 = 2$ K $< T_{\text{f2}}$ deeply inside the spin glass phase, (2) $T_1 = 20$ K in the upper magnetic phase, and (3) $T_1 = 100$ K in the paramagnetic phase. At each T_1, aging for $t_w = 60$ min was employed and the TRM decay was monitored for a time $t \approx 180$ min after the H_{fc} switch-off. The TRM decay curves normalized to the magnetization before the field was cut to zero, $M_{\text{TRM}}(T_1, t)/M_{\text{fc}}(T_1)$, are displayed in Fig. 6. All TRM decays are logarithmically slow in time t. Although it is straightforward to associate the TRM decays within the magnetic phases below 32 K with the slow reorientational dynamics of the correlated spins, it is somewhat surprising that the slow TRM decay also is observed in the paramagnetic phase. The relatively large TRM fraction in the fc magnetization at $T_1 = 100$ K, amounting to $M_{\text{TRM}}(T_1, t = 0)/M_{\text{fc}}(T_1) \approx 0.60$, results from the smallness of the paramagnetic magnetization at this temperature. The magnetically correlated spin fraction responsible for the slow TRM decay within the paramagnetic phase is the one that also produces the zfc–fc susceptibility splitting up to room temperature (Fig. 2(a)). A likely explanation is found in the small FM (or superparamagnetic) iron-rich clusters located at the surfaces of the cracks in the material.

1. Thermoremanent magnetization versus aging time t_w

The TRM-decay experiments as a function of the aging time t_w were performed at $T_1 = 5$ K in the spin glass phase. The sample was field cooled in $H_{\text{fc}} = 8$ Oe and was aged in this field at T_1 for $t_w = 0, 10, 15, 30, 45, 60, 120, 240,$ and 360 min. After $H_{\text{fc}} \to 0$, the TRM time decays were monitored up to $t = 180$ min. The normalized TRM decays as a function of the aging time t_w, $M_{\text{TRM}}(t_w, t)/M_{\text{fc}}(t_w)$, are shown in Fig. 7(a). The normalized TRM magnitude (the TRM fraction in M_{fc}) increases for increasing t_w. For longer t_w, the decays slow down and the remanence increases. This is also evident from Fig. 7(b), where the normalized TRM values taken at the decay time $t = 40$ min are plotted as a function of t_w.

Remarkably small variations of the TRM decays are depicted in Fig. 7, which are on the order of a couple of tenths of a percent over the decay time of 180 min. At $T_1 = 5$ K, the TRM is composed of two contributions: the spin glass contribution and the contribution of the remnant FM magnetization because of defects that also is observed at $T_1 = 100$ K in Fig. 6(c). The
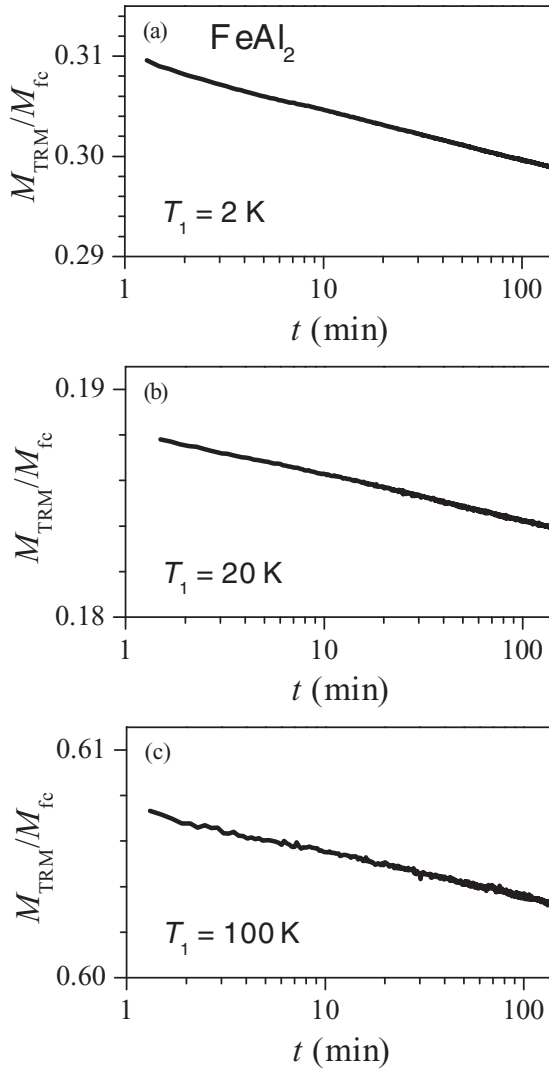
FIG. 6. Normalized TRM time decay M_{TRM}/M_{fc} of FeAl$_2$ at the temperatures (a) $T_1 = 2$ K $< T_{f2}$ deeply inside the spin glass phase, (b) $T_1 = 20$ K in the upper magnetic phase, and (c) $T_1 = 100$ K in the paramagnetic phase. The sample was cooled in the field $H_{fc} = 100$ Oe from room temperature, and aging for $t_w = 60$ min was employed at each T_1 before the field switch-off. All TRM decays are logarithmically slow in time t.

two contributions have quite different decay rates, which can be estimated from Fig. 6 by comparing the magnitudes of the TRM drops over the measured time interval at different temperatures. The TRM decay at $T_1 = 100$ K [Fig. 6(c)] is one order of magnitude slower than the $T_1 = 2$ K decay [Fig. 6(a)]. In the TRM decays as a function of t_w at $T_1 = 5$ K (Fig. 7), the FM contribution can be regarded as approximately constant during the observation time period, so the spin glass part of the TRM decays toward this constant value instead of toward zero. This is the reason for the unusually high $M_{TRM}(t_w,t)/M_{fc}(t_w)$ ratio and the smallness of the TRM variation when the total TRM is plotted as a function of t_w.

2. Thermoremanent magnetization versus cooling field H_{fc}

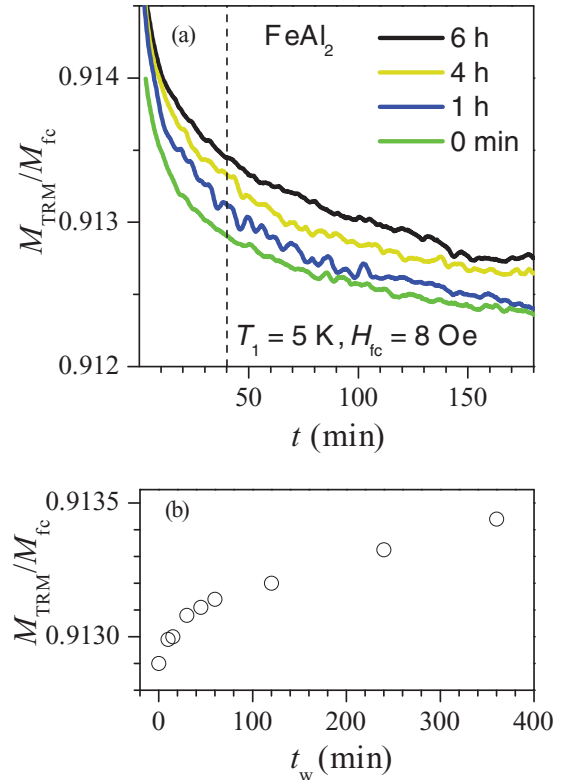In the next set of experiments, the TRM time decay was measured as a function of the cooling field H_{fc} in which

FIG. 7. (Color online) (a) Normalized TRM time decays $M_{TRM}(t_w,t)/M_{fc}(t_w)$ of FeAl$_2$ as a function of the aging time t_w at $T_1 = 5$ K in the spin glass phase. The sample was field cooled in $H_{fc} = 8$ Oe and was aged in this field at T_1 for $t_w = 0$, 10, 15, 30, 45, 60, 120, 240, and 360 min. For clarity, not all t_w curves are shown on the graph. (b) The normalized TRM magnitude, taken from the curves shown in the (a) at the decay time $t = 40$ min (marked by the vertical dashed line), as a function of t_w.

the aging took place. The sample was again field cooled to $T_1 = 5$ K and left there to age for $t_w = 60$ min before the field was cut to zero. The following field values were employed: $H_{fc} = 2$, 4, 8, 50, 200, 500, and 1000 Oe. The TRM decays normalized to M_{fc} are displayed in Fig. 8(a). We observe that $M_{TRM}(H_{fc},t)/M_{fc}(H_{fc})$ decreases strongly with increasing H_{fc}. The normalized TRM amplitude as a function of H_{fc}, taken at the decay time $t = 10$ min, is displayed in Fig. 8(b), where a decrease by a factor of 10 in the field range 2 Oe $< H_{fc} < 1000$ Oe is evident.

The previously presented TRM dependence on the aging time t_w and the cooling field H_{fc} at $T_1 = 5$ K in the spin glass phase originates from the out-of-equilibrium dynamics of a nonergodic spin system that approaches thermal equilibrium within two subsequent time intervals in one TRM-decay experiment. During the aging interval (waiting for t_w in a field H_{fc}), the system approaches an equilibrium state with nonzero magnetization M_{fc} in a field H_{fc}. After the field is cut to zero, the new thermodynamic equilibrium becomes a state with zero magnetization in $H_{fc} = 0$ and the spin system proceeds toward this state during the decay time interval t. In both cases, thermal equilibrium can never be reached on the experimental time scale because of the macroscopic spin relaxation times involved for the spin reorientations. A detailed
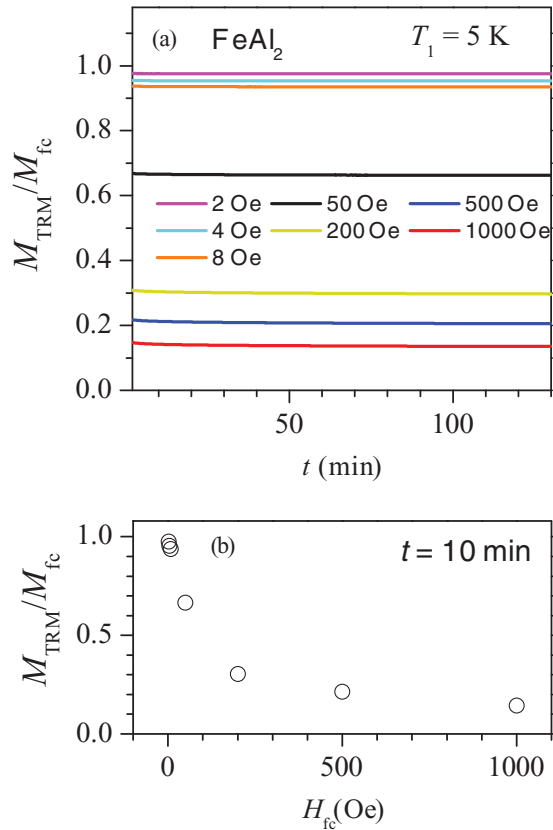
FIG. 8. (Color online) (a) Normalized TRM time decays $M_{TRM}(H_{fc},t)/M_{fc}(H_{fc})$ of FeAl$_2$ as a function of the cooling field H_{fc}. The sample was field cooled to $T_1 = 5$ K in the spin glass phase and aged there in the fields $H_{fc} = 2, 4, 8, 50, 200, 500,$ and 1000 Oe for $t_w = 60$ min before the field was cut to zero. (b) The normalized TRM amplitude as a function of H_{fc}, taken from the curves shown in (a) at $t = 10$ min.

discussion of this phenomenon for a canonical spin glass in terms of the ultrametrically organized free energy landscape, where degenerate metastable states are separated by barriers that are crossed by thermally assisted spin reorientations, can be found elsewhere.[21] An important conclusion of the TRM-decay experiments in the spin glass phase of FeAl$_2$ is that the TRM behaves as a function of t_w and H_{fc} in the same way as in the canonical spin glasses.

F. Discussion

The FeAl$_2$ intermetallic phase undergoes complex two-step magnetic ordering at low temperatures. At $T \approx 32$ K, an inflection-point-type anomaly is observed in χ_{zfc} and χ_{fc}. Below the anomaly temperature, the zfc–fc susceptibility splitting increases rather suddenly, but it remains small and almost temperature independent down to the maximum in χ_{zfc} at 12 K. The ac susceptibility did not reveal any frequency shift of the anomaly temperature. This indicates that at $T \approx 32$ K, a kind of thermodynamic magnetic phase transition (not yet specified) takes place, in which a small fraction of the Fe spins participate. At $T_{f2} \approx 12$ K, a typical spin-freezing transition to a spin glass phase is observed, characterized by a frequency-dependent cusp in the ac susceptibility, a continuously increasing zfc–fc susceptibility splitting below

the cusp temperature, a significant $M(H)$ hysteresis inside the spin glass phase, and the TRM behavior as a function of the aging time t_w and the cooling field H_{fc} typical of canonical spin glasses. From the magnetic structure point of view, our results are compatible with the following physical picture: the majority fraction of Fe spins participates in the spin glass transition at the spin freezing temperature $T_{f2} \approx 12$ K, whereas the minority spin fraction (with considerably stronger interspin exchange interactions) already orders magnetically at a higher temperature $T \approx 32$ K. In the following, we discuss the origin of magnetic frustration and spin glass ordering in the FeAl$_2$ phase by considering structural features of the FeAl$_2$ lattice.

Magnetic frustration leading to a spin glass phase is encountered in spin systems that possess (1) frustration (the interaction between spins is such that no configuration can simultaneously satisfy all bonds and minimize the energy at the same time) and (2) randomness (the spins must be positioned randomly in the material).[23] These two properties lead to highly degenerate free-energy landscapes with a distribution of barriers between different metastable states, resulting in broken ergodicity below the spin-freezing temperature T_f. In FeAl$_2$, the randomness criterion is fulfilled by the three lattice sites M1, M2, and M3 with the mixed Al and Fe occupation in the proportion 0.67Al + 0.33Fe. Each of the three M-type sites is occupied by a magnetic Fe ion with the probability 0.33, the remaining 0.67 being the probability of occupation by a nonmagnetic Al atom. The spins are thus positioned randomly on the M-type sites. The sublattice of iron atoms and mixed-occupation sites is displayed in Fig. 9(a) for the view along the crystallographic a axis; in Fig. 9(b), the same sublattice is shown along the b axis. If all mixed-occupation sites were occupied by the nonmagnetic Al atoms only, the Fe atoms would then form pairs and linearlike triads of direct-coupled spins. A detail of the sublattice, containing each of the five nonequivalent Fe atoms (Fe1–Fe5) and the three nonequivalent mixed sites (M1–M3) of the unit cell only once is displayed in Fig. 9(c). The nearest-neighbor distances are also indicated, ranging between 2.48 and 3.18 Å. In the case that a given M site is occupied by an Fe atom, the nearest-neighbor spins are then located on triangles. Because the coupling between the spins is an AFM type (as evidenced from the negative Curie-Weiss temperature), the spins on the triangles are in a frustrated configuration (all three spins cannot orient antiparallel with respect to both neighbors) for geometric reasons. Both randomness and frustration are thus present on the Fe sublattice of FeAl$_2$. Considering the cluster of Fig. 9(c), the probability of finding a cluster with none of the three M sites occupied by a magnetic Fe is 0.30, the probability of having one Fe and two Al on the M sites is 0.44, the configuration of two Fe and one Al has the probability 0.22, and the three-Fe configuration probability is 0.04. The more Fe atoms on the mixed sites, the more nearest-neighbor spins are located on the triangles.

Considering the entire Fe–M sublattice, there exist Fe-richer and Fe-poorer regions, according to which of the four cluster types is realized more frequently. Cooling down the FeAl$_2$ material results in the freezing of spin reorientation over a broad temperature range and the spin glass ordering of spins in a frustrated configuration. The microscopic origin of the spin glass phase in FeAl$_2$ is thus random positioning of
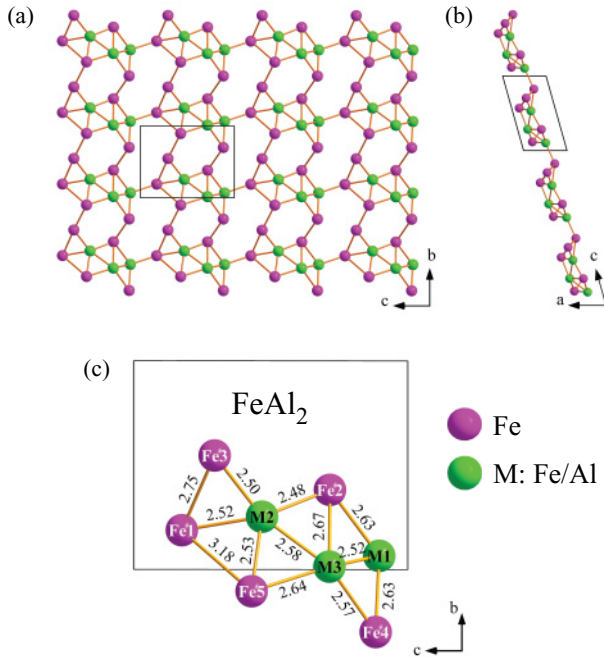
FIG. 9. (Color online) The sublattice of iron atoms and mixed-occupation sites of FeAl$_2$ according to the structural model by Stein *et al.*[14] (a) A view along the *a* crystallographic axis. (b) A view along the *b* axis. (c) A detail of the sublattice, containing each of the five nonequivalent Fe atoms (Fe1–Fe5) and the three nonequivalent mixed sites (M1–M3) of the unit cell only once. The nearest-neighbor distances (in angstrom units) are also indicated. The boxes denote the unit cell.

the Fe spins on the three mixed-occupation sites of the unit cell and geometrical frustration because of positioning of the AFM-coupled spins on triangles. The preceding considerations explain the formation of the spin glass phase below $T_{f2} \approx 12$ K, in which the majority of Fe spins participate. The microscopic origin of magnetic ordering at the higher transition at $T \approx 32$ K, in which only a small fraction of the Fe spins is involved, is less clear. It seems plausible to ascribe this phenomenon to the Fe-richest regions in the material, where the interspin interactions are strong enough to form localized magnetically ordered "droplets" of the Fe spins at a temperature higher than the spin glass transition in the Fe-poorer regions. This is corroborated by the probability of finding an Fe-rich cluster of Fig. 9(c) in the structure (with all three M sites containing an Fe atom) being only 4%, whereas the summed probability of the Fe-poorer clusters (containing two, one, or no Fe atom) is 96%.

IV. IV. MAGNETIC PROPERTIES OF Fe$_2$Al$_5$

A. Zero-field-cooled and field-cooled magnetic susceptibilities

Magnetic properties of Fe$_2$Al$_5$ were determined by the same set of experiments as applied previously to FeAl$_2$. The zfc and fc dc magnetic susceptibilities $\chi = M/H$ of Fe$_2$Al$_5$ in the temperature range 1.9–300 K and magnetic fields $H = 8$, 50, and 100 Oe and $H = 1$ and 10 kOe are shown in Fig. 10(a). The zfc–fc susceptibility splitting up to room
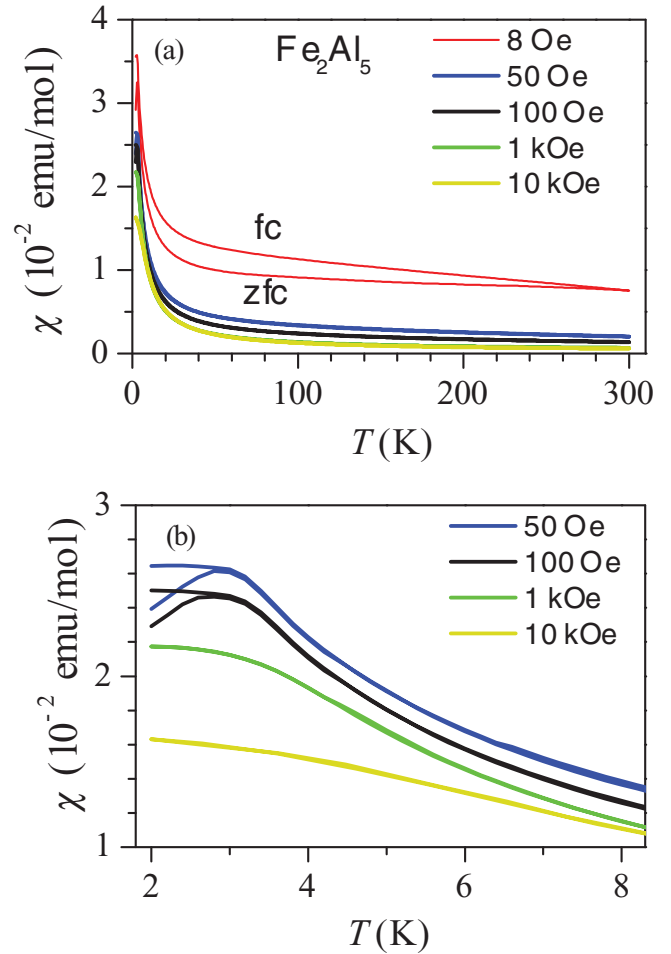

FIG. 10. (Color online) (a) The zfc and fc dc magnetic suscepti-bilities $\chi = M/H$ of Fe$_2$Al$_5$ in the temperature range 1.9–300 K in magnetic fields $H = 8$, 50, and 100 Oe and $H = 1$ and 10 kOe. (b) χ_{zfc} and χ_{fc} on an expanded scale below 8 K.

temperature is visible for the lowest field of 8 Oe, whereas it becomes unobservable on the scale of Fig. 10(a) for the higher fields investigated. This tiny splitting again occurs because of a small fraction of magnetically ordered Fe spins that can presumably be associated with defects in the material (Fe-rich spin clusters at the surface of the cracks and/or FM surface iron oxides). χ_{zfc} and χ_{fc} are shown on an expanded scale below 8 K in Fig. 10(b) (except for the lowest field of 8 Oe). Additional zfc–fc splitting and a cusp in χ_{zfc} appear at 3 K for the low fields up to 100 Oe, whereas at higher fields of 1 and 10 kOe the splitting has already been destroyed by the magnetic field. The field-induced destruction of the zfc–fc susceptibility splitting below 3 K shows that the internal magnetic structure is "soft" and fragile with respect to the external magnetic field, which is already at a strength on the order of 100 Oe. The cusp in χ_{zfc} at low magnetic fields, the continuously increasing zfc–fc susceptibility splitting, and the temperature-independent χ_{fc} below the cusp temperature allow this temperature to be associated with the spin-freezing temperature $T_f \approx 3$ K and classification of the low-temperature phase of Fe$_2$Al$_5$ as a spin glass phase. The spin glass phase in Fe$_2$Al$_5$ was not reported previously in the literature. In a recent study,[8] the magnetic susceptibility of Fe$_2$Al$_5$ was
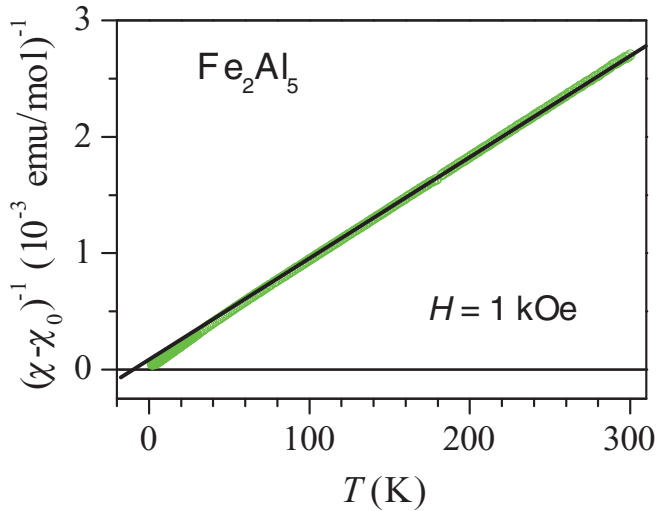
FIG. 11. (Color online) Magnetic susceptibility of Fe_2Al_5 in $H = 1$ kOe in a $(\chi - \chi_0)^{-1}$ versus temperature plot. The solid line is the Curie-Weiss fit with Eq. (1) of the high-temperature data $T > 80$ K. The fit parameters are given in the text.

investigated in the magnetic field $H = 1$ kOe and Curie-Weiss paramagnetism was reported down to the lowest investigated temperature. This result is in agreement with our susceptibility data in the field $H = 1$ kOe, which is already strong enough to destroy the zfc–fc susceptibility splitting and polarize the fragile internal magnetic (spin glass) structure. The spin glass phase in Fe_2Al_5 can only be observed in low magnetic fields below ~100 Oe and is missed in experiments employing magnetic fields of $H = 1$ kOe and higher.

B. Paramagnetic susceptibility

The analysis of the susceptibility $\chi(T)$ of Fe_2Al_5 in the high-temperature paramagnetic regime was performed with the Curie-Weiss law of Eq. (1). The high-temperature data for $T > 80$ K of the susceptibility measured in the field $H = 1$ kOe were used. The $(\chi - \chi_0)^{-1}$ versus temperature plot is shown in Fig. 11. The fit (solid line) yielded the parameter values $\chi_0 = 3.1 \times 10^{-4}$ emu/mol, $C = 0.11$ emu K/mol, and $\theta = -6.4$ K. The negative Curie-Weiss temperature suggests a prevailing AFM-type coupling between the spins. The Larmor diamagnetic susceptibility χ_{dia} was calculated to be in the range $\chi_{dia} = (-3.0, -3.6) \times 10^{-5}$ emu/mol. The fit-determined χ_0 value is 10 times larger than $|\chi_{dia}|$, confirming that a small FM contribution is present in the signal of the paramagnetic phase. The mean effective Bohr magneton number was calculated from the Curie constant to be $\bar{p}_{eff} = 0.7$ per Fe atom, demonstrating that the Fe moments in the Fe_2Al_5 phase are partially screened by the conduction-electron cloud in a conducting environment. The smaller Bohr magneton number ($\bar{p}_{eff} = 0.7$) and the less negative Curie-Weiss temperature ($\theta = -6.4$ K) of Fe_2Al_5, as compared to $FeAl_2$ (where $\bar{p}_{eff} = 2.9$ and $\theta = -35$ K), suggest weaker interspin coupling in the former compound. This is in agreement with the lower spin freezing temperature $T_f \approx 3$ K of Fe_2Al_5, as compared to $T_{f2} \approx 12$ K of $FeAl_2$. The FM spin fraction in the high-temperature paramagnetic

phase of Fe_2Al_5 is also about 10 times smaller than in $FeAl_2$. Because Fig. 1(a) and (b) show that the density of cracks in Fe_2Al_5 is considerably smaller than in $FeAl_2$, associating the FM signal with the surface defects in these compounds (Fe-rich spin clusters at the surface of the cracks and/or FM surface iron oxides) seems likely.

C. Ac susceptibility

The real part χ' of the ac susceptibility of Fe_2Al_5, measured in an ac magnetic field of amplitude $H_0 = 6.5$ Oe at the frequencies $\nu = 1, 10, 100$, and 1000 Hz, is shown in Fig. 12(a). χ' shows a frequency-dependent cusp at $T \approx 3$ K that shifts to lower temperatures at lower frequencies. The zoomed-in part of the frequency-dependent cusp is shown in the inset of Fig. 12(a). By considering the cusp in χ' as though it occurred at the spin-freezing temperature T_f, below which the ergodicity of the spin system is broken on the experimental time scale, the $T_f(\nu)$ relation was determined from the $\chi'(\nu)$ curves. The $T_f(\nu)$ graph is shown in Fig. 12(b), where a logarithmic dependence (base 10) on the frequency is evident. At the lowest frequency the cusp occurs at the temperature $T_f(1\ Hz) = 3.1$ K, whereas at the highest frequency it occurs at $T_f(1\ kHz) = 3.3$ K. The relative change of T_f per decade ν is $\Delta T_f/T_f \Delta (\log \nu) = 0.024$, which is in the range found for canonical spin glasses[20] and very close to the value (0.028) found for T_{f2} in $FeAl_2$. This
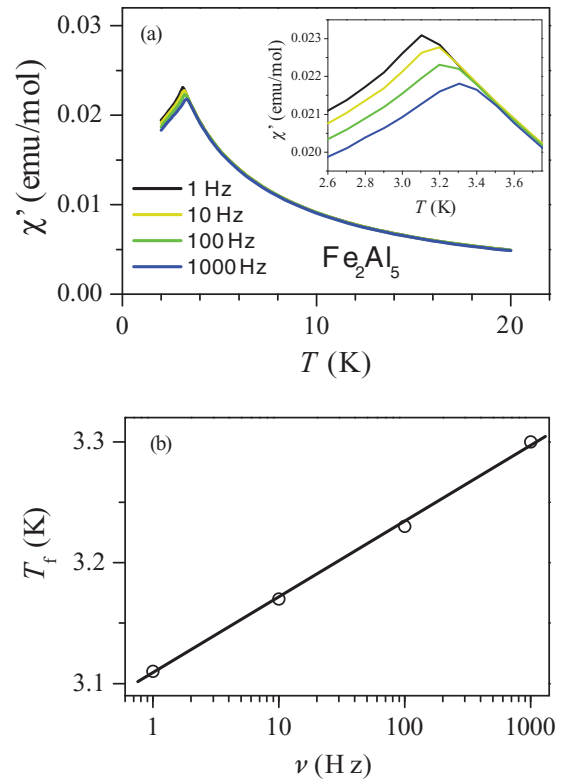

FIG. 12. (Color online) (a) Real part χ' of the ac susceptibility of Fe_2Al_5 measured in an ac magnetic field of amplitude $H_0 = 6.5$ Oe at frequencies $\nu = 1, 10, 100$, and 1000 Hz. The zoomed-in part of χ' around the frequency-dependent cusp is shown in the inset. (b) Frequency dependence of the temperature T_f of the maximum in χ'. A solid line was used to evaluate the relative change of T_f per decade ν, $\Delta T_f/T_f \Delta (\log \nu) = 0.024$.
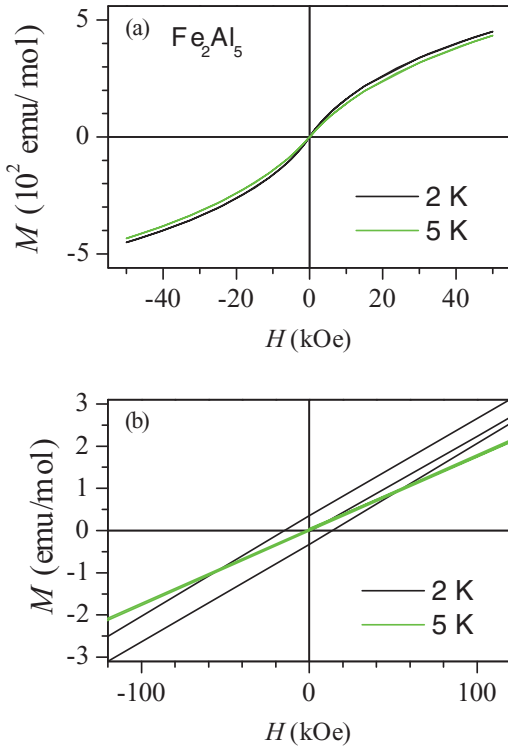
FIG. 13. (Color online) (a) $M(H)$ curves of Fe_2Al_5 at $T = 2$ and 5 K for the field sweep $\pm$ 50 kOe. (b) The zoomed-in parts of the hysteretic region around $H = 0$.

classifies the spin-freezing transition in Fe_2Al_5 at $T_f \approx 3$ K as being of spin glass type.

D. Magnetization versus magnetic field

The $M(H)$ curves of Fe_2Al_5 were recorded at $T = 2$ K in the spin glass phase and $T = 5$ K just above T_f (Fig. 13(a)). The shape of both curves is similar, showing curvature typical of localized magnetic moments superposed on a linear contribution. The main difference between the two curves is the hysteretic region around $H = 0$ (Fig. 13(b)). The $T = 2$ K curve shows small but significant hysteresis with the coercive field $H_c^{2K} = 14.5$ Oe, whereas no pronounced hysteresis could be observed at 5 K (except for a tiny hysteresis with $H_c^{5K} \approx 1$ Oe that is comparable to the remanence of the employed superconducting magnet). Hysteretic behavior of the spin system is thus observed only below the spin freezing temperature T_f. The magnetic field where the $M(H)$ hysteresis loop at $T = 2$ K closes up is difficult to determine reliably because of the smallness of the coercive field.

E. Thermoremanent magnetization

The TRM time decay of Fe_2Al_5 after cooling in the field $H_{fc} = 100$ Oe and aging for $t_w = 60$ min before the field cutoff was recorded at the measuring temperatures $T_1 = 2$ K $< T_f$ in the spin glass phase and $T_1 = 3, 4,$ and 5 K just above the spin glass phase. Although there exists significant TRM at $T_1 = 2$ K that decays logarithmically slowly in time t (Fig. 14), no TRM was detected at 3 K and higher. The tiny nonzero constant value of $M_{TRM}(T_1,t)/M_{fc}(T_1) = 0.05$ at $T_1 = 3$ K
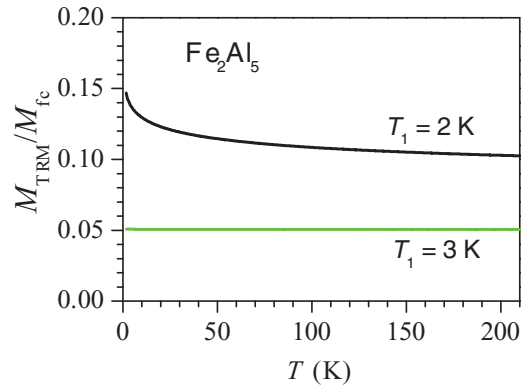

FIG. 14. (Color online) Normalized TRM time decays M_{TRM}/M_{fc} of Fe_2Al_5 at the temperatures $T_1 = 2$ K $< T_f$ and $T_1 = 3$ K $\approx T_f$. The sample was cooled in the field $H_{fc} = 100$ Oe from room temperature, and aging for $t_w = 60$ min was employed before the field switch-off. The tiny nonzero constant value of $M_{TRM}(T_1,t)/M_{fc}(T_1) = 0.05$ at $T_1 = 3$ K results from the small FM magnetization in the paramagnetic phase.

results from the aforementioned small FM magnetization in the paramagnetic phase.

1. Thermoremanent magnetization versus aging time t_w

The TRM-decay experiments as a function of the aging time t_w were performed at $T_1 = 2$ K in the spin glass phase. The sample was field cooled in $H_{fc} = 8$ Oe and was aged in this field at T_1 for $t_w = 0, 5, 10, 15, 30, 45, 120, 240,$ and 360 min. The normalized TRM decays as a function of the aging time t_w, $M_{TRM}(t_w,t)/M_{fc}(t_w)$, are shown in Fig. 15(a). A typical spin glass behavior is observed, where the normalized TRM magnitude increases for increasing t_w. This is also evident from Fig. 15(b), where the normalized TRM values, taken at the decay time $t = 40$ min, are plotted as a function of t_w.

2. Thermoremanent magnetization versus cooling field H_{fc}

In the last set of experiments, the TRM time decay was measured as a function of the cooling field H_{fc}. The sample was again field cooled to $T_1 = 2$ K in the spin glass phase and left there to age for $t_w = 60$ min before the field was cut to zero. The following field values were employed: $H_{fc} = 2, 50, 100, 200, 500,$ and 1000 Oe. The TRM decays normalized to M_{fc} are displayed in Fig. 16(a). We observe a typical spin glass behavior, where $M_{TRM}(H_{fc},t)/M_{fc}(H_{fc})$ decreases strongly with increasing H_{fc}. The normalized TRM amplitude as a function of H_{fc}, taken at the decay time $t = 40$ min, is displayed in Fig. 16(b), where a decrease by a factor of 22 in the field range 2 Oe $< H_{fc} <$ 1000 Oe is evident.

F. Discussion

The Fe_2Al_5 intermetallic phase shows a spin-freezing transition to a spin glass phase at $T_f \approx 3$ K, characterized by a frequency-dependent cusp in the ac susceptibility, a continuously increasing zfc–fc susceptibility splitting below the cusp temperature, a temperature-independent χ_{fc} below the cusp temperature, a significant $M(H)$ hysteresis inside the spin glass phase, and the TRM behavior as a function of the aging time t_w and the cooling field H_{fc} typical of canonical spin glasses. The spin glass phase in Fe_2Al_5 is "soft" and fragile
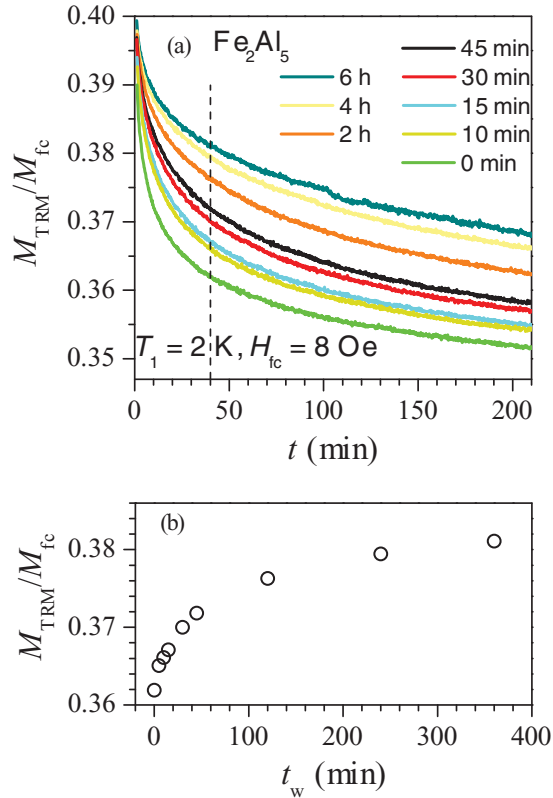
FIG. 15. (Color online) (a) Normalized TRM time decays $M_{TRM}(t_w,t)/M_{fc}(t_w)$ of Fe$_2$Al$_5$ as a function of the aging time t_w at $T_1 = 2$ K in the spin glass phase. The sample was field cooled in $H_{fc} = 8$ Oe and was aged in this field at T_1 for $t_w = 0, 5, 10, 15,$ 30, 45, 120, 240, and 360 min. (b) The normalized TRM amplitude, taken from the curves shown in (a) at the decay time $t = 40$ min, as a function of t_w.

FIG. 16. (Color online) (a) Normalized TRM time decays $M_{TRM}(H_{fc},t)/M_{fc}(H_{fc})$ of Fe$_2$Al$_5$ as a function of the cooling field H_{fc}. The sample was field cooled to $T_1 = 2$ K in the spin glass phase and aged there in the fields $H_{fc} = 2, 50, 100, 200, 500,$ and 1000 Oe for $t_w = 60$ min before the field was cut to zero. (b) The normalized TRM amplitude as a function of H_{fc}, taken from the curves shown in (a) at $t = 40$ min.

with respect to the external magnetic field and can only be observed in low magnetic fields below ~100 Oe.

To reveal the origin of magnetic frustration and spin glass ordering in the Fe$_2$Al$_5$ phase, we search for the randomness and frustration within the Fe spin system by considering structural features of the lattice. In the Fe$_2$Al$_5$ unit cell,[15] the single Fe crystallographic site is fully occupied, so the spins are not positioned randomly in the structure. Each Fe atom has two somewhat distant Fe near-neighbors (3.06Å), as well as eight Al1 neighbors and a series of partially occupied Al2 and Al3 sites (occupation factors of 0.36 and 0.23), making up disordered chains along [001]. The partially occupied sites introduce a certain degree of randomness in the local environments of the Fe atoms. Because the local near-neighbor coordination by the Al atoms determines the amount of screening of the Fe magnetic moment by the surrounding electron cloud, randomness in the local environments introduces random distribution of the sizes of the magnetic moments over the Fe sublattice. The partial screening of the Fe moments in the Fe$_2$Al$_5$ phase is experimentally supported by the strongly reduced value of the mean effective Bohr magneton number ($\bar{p}_{eff} = 0.7$ per Fe atom), as determined from the Curie-Weiss analysis of the paramagnetic susceptibility. Therefore, although the spins are not positioned randomly in the Fe$_2$Al$_5$ structure, randomness in the local chemical environments of the Fe sites because
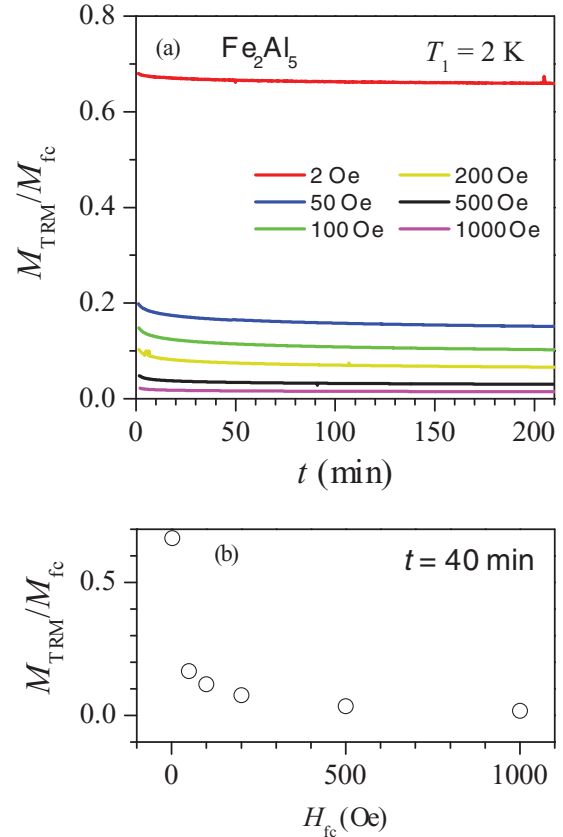
of the partial occupation of the neighboring Al2 and Al3 sites imposes random distribution of the magnetic moment sizes and the interspin coupling constants. Randomness is thus present on the Fe sublattice. Geometric frustration because of the distribution of the AFM-coupled nearest-neighbor spins on triangles is present in Fe$_2$Al$_5$ as well (where the AFM-type coupling follows from the negative value of the Curie-Weiss temperature). In Fig. 17(a), the Fe sublattice of the Fe$_2$Al$_5$ structure is shown, where the Fe atoms form infinite triangular chains in the [001] direction. Because all of the Fe atoms are located on the triangular chains, all spins of the structure are in a frustrated configuration because of geometrical reasons. In Fig. 17(b), the Fe triangular chains are viewed along [100] with the nearest-neighbor distances indicated. The Fe–Fe distances on the isosceles triangles are relatively large (two times 3.06 Å and one 4.22Å), imposing relatively weak direct contacts between the spins. This is reflected in the low spin-freezing temperature $T_f \approx 3$ K and the fragileness of the spin glass structure that is already destroyed and polarized by the external magnetic field as low as 1 kOe. Random distribution of the magnetic moment sizes and the interspin coupling constants on the Fe sublattice, as well as the geometrical frustration of
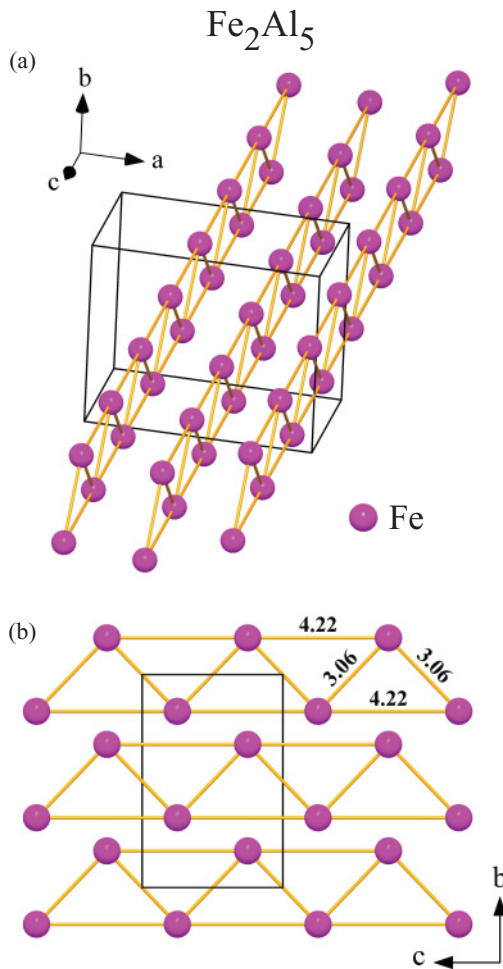
FIG. 17. (Color online) (a) The Fe sublattice of the Fe_2Al_5 structure according to the model by Burkhardt *et al.* (Ref. 15). The Fe atoms form infinite triangular chains in the [001] direction. (b) The Fe triangular chains viewed along [100] with the Fe–Fe distances (in angstrom units) indicated. The boxes denote the unit cell.

the AFM-coupled spins on triangles, is at the origin of the spin glass phase in Fe_2Al_5.

V. CONCLUSIONS

In this work, we revisited the magnetic properties of the $FeAl_2$ and Fe_2Al_5 intermetallic compounds in the aluminum-rich side of the Fe–Al phase diagram. We found that the magnetic structures of the investigated compounds are richer than published so far in the literature. $FeAl_2$ undergoes complex two-step magnetic ordering at low temperatures. At $T \approx 32$ K, a magnetic phase transition (not yet specified) takes place in which a small fraction of the Fe spins participate, whereas at $T_{f2} \approx 12$ K, the majority spin fraction undergoes a spin-freezing transition to a spin glass phase. This is in contrast to the previous studies that have reported a single transition to a spin glass phase at the spin freezing temperature $T_f = 35$ K. The microscopic origin of the spin glass phase in the structurally well-ordered $FeAl_2$ is random positioning of the Fe spins on the three mixed-occupation Al/Fe sites of the unit cell and the geometrical frustration because of positioning of the AFM-coupled spins on triangles. The origin of magnetic ordering at the higher transition at $T \approx 32$ K, in which only a small fraction of the Fe spins is involved, is less clear, but it is plausible to ascribe this phenomenon to the Fe-richest regions in the material, where the interspin interactions are strong enough to form localized magnetically ordered "droplets" of the Fe spins already at a temperature higher than the spin glass transition in the Fe-poorer regions. This is corroborated by the probability of finding an Fe-rich cluster in the $FeAl_2$ structure (with all three mixed-occupation sites containing an Fe atom) being only 4%, whereas the summed probability of the Fe-poorer clusters (containing two, one, or no Fe atom on the mixed-occupation sites) is 96%.

The Fe_2Al_5 intermetallic phase shows a transition to a spin glass phase at the spin freezing temperature $T_f \approx 3$ K, which was not reported previously. The spin glass phase is "soft" and fragile with respect to the external magnetic field and can only be observed in low magnetic fields below ~ 100 Oe. In searching for the randomness and frustration of the spin system that lead to the spin glass ordering, we found that all sites of the Fe sublattice are fully occupied, so the spins are not positioned randomly in the Fe_2Al_5 structure. However, randomness in the local chemical environments of the Fe sites because of the partial occupation of the neighboring Al2 and Al3 sites imposes different degrees of Fe moment screening by the conduction-electron cloud, resulting in a random distribution of the magnetic moment sizes and the interspin coupling constants. Geometric frustration because of the distribution of the AFM-coupled nearest-neighbor spins on triangles is present as well. Thus, randomness and frustration are both present in the structurally well-ordered Fe_2Al_5 phase.

*jani.dolinsek@ijs.si

[1] D. Guenzburger and D. E. Ellis, Phys. Rev. Lett. **67**, 3832 (1991).

[2] P. G. Gonzales, L. A. Terrazos, H. M. Petrilli, and S. Frota-Pessôa, Phys. Rev. B **57**, 7004 (1998).

[3] P. Shukla and M. Wortis, Phys. Rev. B **21**, 159 (1980).

[4] W. Bao, S. Raymond, S. M. Shapiro, K. Motoya, B. Fak, and R. W. Erwin, Phys. Rev. Lett. **82**, 4711 (1999).

[5] C. S. Lue, Y. Öner, D. G. Naugle, and J. H. Ross, Jr., Phys. Rev. B **63**, 184405 (2001).

[6] J. Chi, Y. Li, F. G. Vagizov, V. Goruganti, and J. H. Ross Jr., Phys. Rev. B **71**, 024431 (2005).

[7] F. Müller, M. Rosenberg, W. Liu, and U. Köster, Mater. Sci. Eng. A **134**, 900 (1991).

[8] J. Chi, X. Zheng, S. Rodriguez, Y. Li, W. Gou, V. Goruganti, K. D. D. Rathnayaka, and J. H. Ross Jr., Phys. Rev. B **82**, 174419 (2010).

[9] P. Popčević, A. Smontara, J. Ivkov, M. Wencka, M. Komelj, P. Jeglič, S. Vrtnik, M. Bobnar, Z. Jagličić, B. Bauer, P. Gille, H. Borrmann, U. Burkhardt, Yu. Grin, and J. Dolinšek, Phys. Rev. B **81**, 184203 (2010).

[10] R. N. Corby and P. J. Black, Acta Cryst. B **29**, 2669 (1973).

[11] M. Khaidar, C. H. Allibert, and J. Driole, Z. Metallkd. **73**, 433 (1982).

[12] A. M. Van Der Kraan and K. H. J. Buschow, Physica B+C (Amsterdam) **138**, 55 (1986).

[13] M. Palm, J. Alloys Compd. **252**, 192 (1997).

[14] F. Stein, G. Sauthoff, and M. Palm, Z. Metallkd. **95**, 469 (2004).

[15] U. Burkhardt, Yu. Grin, M. Ellner, and K. Peters, Acta Cryst. B **50**, 313 (1994).

[16] Z. W. Chen, R. M. Sharp, and J. T. Gregory, Mater. Sci. Technol. **6**, 1173 (1990).

[17] U. Köster, B. Schuhmacher, and D. Sommer, Steel Res. **72**, 371 (2001).

[18] R. L. Dutta and A. Syamal, *Elements of Magnetochemistry* (Affiliated East-West Press, New Delhi, 1993), p. 8.

[19] F. E. Mabbs and D. J. Machin, *Magnetism and Transition Metal Complexes* (Chapman and Hall, London, 1973), p. 7.

[20] J. A. Mydosh, *Spin Glasses: An Experimental Introduction* (Taylor & Francis, London, 1993), p. 67.

[21] M. Lederman, R. Orbach, J. M. Hammann, M. Ocio, and E. Vincent, Phys. Rev. B **44**, 7403 (1991).

[22] D. Chu, G. G. Kenning, and R. Orbach, Philos. Mag. B **71**, 479 (1995).

[23] K. Binder and A. P. Young, Rev. Mod. Phys. **58**, 801 (1986).